Effective Vessel Recognition in High Resolution SAR Images Using Quantitative and Qualitative Training Data Enhancement From Target Velocity Phase Refocusing

Juyoung Song, *Student Member, IEEE*, Duk-jin Kim, *Senior Member, IEEE*, Ji-Hwan Hwang, Hwisong Kim, *Student Member, IEEE*, Chenglei Li, *Student Member, IEEE*, Shinhye Han, and Junwoo Kim

***Abstract*— Along with vessel detection, vessel recognition in high-resolution SAR images was necessary in order to monitor marine vessels effectively; however, the lack of target data and phase defocusing of the target from its velocity limited the recognition performance, especially when using detectors based on artificial intelligence. This study accordingly proposed effective vessel recognition in high-resolution ICEYE spotlight SAR images consecutively using 1) vessel detector robust to defocused moving vessels and 2) mitigation of moving target phase distortion. In order to apply quantitative and qualitative training data enhancement, a target velocity SAR phase refocusing function was developed. The proposed target velocity SAR phase refocusing function generated a defocused SLC image with respect to different target azimuth velocities, which can be used for both training data augmentation and refocusing of velocity-induced phase distortion. Achievement of stable vessel recognition performance was enabled by 1) robust vessel detection on defocused moving vessels and 2) well-focused detected vessel targets, both of which were consecutively applied using the proposed target velocity SAR phase refocusing function. Vessel detection results demonstrated robust performance regardless of vessel motion, and vessel recognition results significantly improved after phase refocusing, both of which were subject to quantitative and qualitative training data enhancement. The performance of the proposed algorithm was analyzed both in terms of phase focusing and velocity estimation. Refocusing performance outperformed that of conventional state-of-the-art autofocusing algorithm, modified Phase Gradient Autofocusing, while azimuth velocity estimation derived the average offset of 0.68 m/s, which was regarded more accurate than previous azimuth velocity estimators based on single-channel SAR image.**

Manuscript received 6 August 2023; revised 22 October 2023 and 5 December 2023; accepted 12 December 2023. Date of publication 22 December 2023; date of current version 11 January 2024. This work was supported in part by the National Research Foundation of Korea (NRF) through the Korea Government (MSIT) under Grant 2021R1A2C2006025, in part by the Korea Institute of Marine Science and Technology Promotion (KIMST) through the Korea Coast Guard under Grant RS-2023-00238652, and in part by Integrated Satellite-Based Applications Development for Korea Coast Guard. *(Corresponding author: Duk-jin Kim.)*

Juyoung Song, Duk-jin Kim, Hwisong Kim, Chenglei Li, and Junwoo Kim are with the School of Earth and Environmental Sciences, Seoul National University, Seoul 08826, South Korea (e-mail: 96daniel@snu.ac.kr; djkim@snu.ac.kr; rlagnlthd1@snu.ac.kr; sengrea0926@snu.ac.kr; darkcroa@snu.ac.kr).

Ji-Hwan Hwang is with EchoSensing Inc., Suwon 16512, South Korea (e-mail: hwang1651@naver.com).

Shinhye Han is with the Interdiciplinary Program in Artificial Intelligence, Seoul National University, Seoul 08826, South Korea (e-mail: sienna.shhan@snu.ac.kr).

Digital Object Identifier 10.1109/TGRS.2023.3346171

***Index Terms*— Automatic identification system (AIS), phase refocusing, SAR, vessel detection, vessel recognition.**

I. Introduction

STABLE monitoring of marine vessels was regarded as essential for maritime safety, which was often conducted using weather-independent SAR image data [1]. Monitoring of marine vessels was widely applied using single or multi-class vessel detection [2]. Different marine vessel detectors were developed, from algorithms based on Constant False Alarm Rate (CFAR) [3], [4] to Convolutional Neural Networks (CNN) [5], [6]. In contrast to CFAR detectors and their variations, CNN analyzed the target pattern and its pixel arrangement using a repetitive convolution calculator [7]. Given that the vessel backscattering signature in SAR was presented as a summation of different targets in each pixel [8], the application of a CNN-based detector in SAR image was able to be regarded effective in aspect of the robustness, especially when discriminating vessel-like targets in coastal regions: bridges, buoys, and small islands [9].

In order to use CNN-based detectors for vessel monitoring, the acquisition of accurate training data was decisive in performance enhancement [10]. SAR image chip database containing vessel signature was presented, which could be used as training data: OpenSARShip [11]; moreover, automated acquisition of training data of vessels from real-time vessel information, Automatic Identification System (AIS), was demonstrated [12]. In the case of handling low-resolution images, which include a number of vessels in the scene, such acquisition methods would be effective. For high-resolution SAR images with a small number of vessels and regions of interest, the generation of the training database was, however, limited; stable vessel detection, recognition and application were accordingly limited. Notably, vessel recognition with multiple classes was rarely conducted from high-resolution SAR images due to insufficient training data [13], [14]. Data augmentation was able to be applied, not all of which represented the practical acquisition geometry of SAR data [15].

In the case where the target moves with significant velocity in SAR coverage, the Doppler effect, furthermore, distorted

target position and phase [16], [17], [18]; range projection of velocity shifted the target, while azimuth projection defocused the phase in azimuth direction. Azimuth defocusing distorted the backscattering characters of vessels significantly, and accordingly, the detection performance, while its enhancement was yet to be analyzed. Hence, in order to develop a stable vessel recognition algorithm for marine vessel surveillance, not only the augmentation of vessel training data but also the calibration of SAR azimuth defocusing from vessel velocity was essential.

Elimination of SAR phase defocusing from antenna and target motion was previously applied using autofocusing, namely Phase Gradient Autofocus (PGA), Inverse SAR (ISAR) minimum Entropy (ME) Autofocusing and Map-drift (MD) autofocusing algorithm [19], [20], [21]. Although the conventional autofocusing algorithms were effective in restoring well-focused target signatures, the target was required to be detected in advance so that autofocusing could be applied. Without the development of robust vessel detection, phase enhancement of azimuth defocused target was, therefore, limited, along with proper recognition of vessels in different types.

As a remedy, quantitative data enhancement was proposed using AIS information, both from an automatic acquisition algorithm [12] and visual inspection [11]. Despite the assistance of AIS information, which enhanced the reliability and quantity of vessel training data [12], it was insufficient to mitigate the image data scarcity for high-resolution SAR images. Such drawback limited the application of refocusing of vessels, as velocity-defocused vessels were difficult to be detected and recognized. Hence, 1) quantitative data enhancement targeting the detection of velocity-distorted vessels and 2) qualitative data enhancement, which refocuses the detected vessels for subsequent recognition, were essential for effective maritime surveillance, even without the support of AIS information.

In this study, enhancement of vessel recognition performance was demonstrated using a consecutive operation of 1) robust vessel detection to defocused moving vessels and 2) phase refocusing to the detected target vessels for their recognition. In order to apply the two operations consecutively, quantitative and qualitative enhancement of SAR vessel training data was proposed using a target velocity SAR phase refocusing function. Presented target velocity SAR phase refocusing was inversely applied to generate an intentionally defocused image for training the vessel detector and accordingly obtained high vessel detection performance. By targeting the detected vessels, phase refocusing was performed and optimized to achieve well-focused targets, which were then used to train the vessel recognition algorithm. The SAR phase refocusing algorithm in this study not only augments the training data for the detection of defocused vessels but also enhances the detected vessel signature.

This study is organized as follows. In Section II, the target velocity SAR phase refocusing function using different target azimuth velocities is derived from the Range-Doppler Algorithm (RDA). In Section III, the application of the proposed refocusing algorithm to quantitative and qualitative enhancement of vessel training data was, respectively, presented, applied to high resolution spotlight SAR images. The results of applying the proposed workflow are presented in Section IV, while enhancement of the target velocity SAR phase refocusing with respect to the conventional autofocusing algorithm is concretely illustrated in Section V. The concluding remarks are presented in Section VI.

II. Target Velocity SAR Phase Refocusing

The proposed target velocity SAR phase refocusing modified the phase of the SAR image using target azimuth velocity as its initial value. It exploited the fundamental relation of RDA, one of the typical SAR image restoration algorithms [22], [23]. Given that the SAR antenna and the target were initially placed at $(0, 0, H)$ and $(0, y_0, 0)$, the position of those after slow time η is elaborated as Fig. 1. By using the second-order Taylor expansion to the slant range, the SAR range equation can be approximated as (1), where $R_0 = (y_0^2 + H^2)^{1/2}$. Accordingly, its SLC signal after RDA application using (1) is able to be described as (2) [24]. Moving target azimuth and range velocity projection is, respectively, signified as v_x and v_y, range acceleration as a_y, and antenna velocity as v_a. Reference wavelength estimated from carrier frequency f_c is denoted as λ_0. The notations P_1 and P_2, respectively, indicate intensity and coefficient of sinc function

$$R(\eta) = R_0 + \frac{y_0 v_y}{R_0}\eta + \frac{1}{2R_0}((v_a - v_x)^2 + v_y^2\left(1 - \left(\frac{y_0}{R_0}\right)^2\right) + y_0 a_y)\eta^2 \tag{1}$$

$$s_{SLC}(\eta) = P_1 \mathrm{sinc}(P_2\pi)\exp\left(-\frac{4\pi j}{\lambda_0}R_0\right)\exp\left(-\frac{4\pi j}{\lambda_0}\frac{y_0 v_y}{R_0}\eta\right)\exp\left(\frac{2\pi j}{\lambda_0 R_0}\left[(v_a - v_x)^2 + v_y^2\left(1 - \left(\frac{y_0}{R_0}\right)^2\right) + y_0 a_y\right]\eta^2\right). \tag{2}$$

Given that the most decisive factor causing azimuth defocusing in (2) was v_x in quadratic term of η [24], v_y and a_y coefficients were neglected in the SLC phase as in (3). The quantitative influence of the two approximated terms was further analyzed in Section V. Doppler history, derivative of SLC phase is expressed as in (4)

$$\varphi(\eta) \cong -\frac{4\pi}{\lambda_0}R_0 - \frac{4\pi}{\lambda_0}\frac{y_0 v_y}{R_0}\eta + \frac{2\pi}{\lambda_0 R_0}(v_a - v_x)^2\eta^2 \tag{3}$$

$$f_D(\eta) = \frac{1}{2\pi}\frac{\mathrm{d}\varphi(\eta)}{\mathrm{d}\eta} \cong -\frac{2}{\lambda_0}\frac{y_0 v_y}{R_0} + \frac{2}{\lambda_0 R_0}(v_a - v_x)^2\eta. \tag{4}$$

Doppler history $f_D(\eta)$ is illustrated as a green line in Fig. 1(b), whose y-intercept causes position displacement of the imaged target and slope difference causes target phase defocusing. Additional derivative of (4) indicates Doppler rate as in (5), while (6) signifies that for ground target

$$K_a = \frac{\mathrm{d}f_D(\eta)}{\mathrm{d}\eta} \cong \frac{2}{\lambda_0 R_0}(v_a - v_x)^2 \tag{5}$$

$$K_{a,v_x=0} = \frac{2v_a^2}{\lambda_0 R_0}. \tag{6}$$

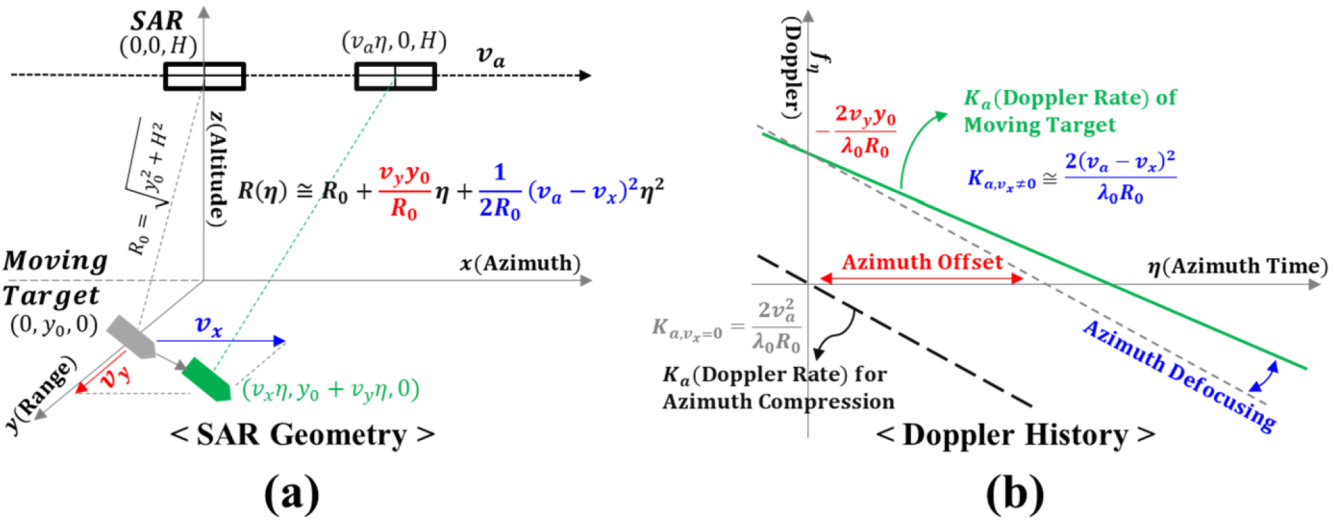

Fig. 1. (a) SAR image acquisition geometry of horizontally moving target and (b) its corresponding Doppler history. Positive target azimuth velocity signifies the target moving against the SAR antenna.

The main idea of target velocity SAR phase refocusing was removing the phase of ground targets and adding the phase of moving targets to the entire SAR SLC image with respect to different target azimuth velocities. The two different phase multipliers were incorporated into a phase compensation filter, as follows:

$$\exp\left(-j\varphi_{\text{comp}}\right) = \exp(j\varphi_{v_x=0})\exp(-j\varphi). \tag{7}$$

The wavelength of the SAR system was subject to range frequency; as the range frequency was modulated using carrier frequency and bandwidth, reference wavelength λ_0 turns into λ_τ as in (8). The notation c_0 denotes the speed of light, while f_τ signifies range frequency deviation. Incorporating (3) and (8), the quadratic phase function in the range frequency-azimuth time domain is derived as in (9)

$$\lambda_\tau = \frac{c_0}{f_c + f_\tau} \tag{8}$$

$$\varphi_2(f_\tau, \eta) = \frac{2\pi}{c_0 R_0}(f_c + f_\tau)(v_a - v_x)^2\eta^2. \tag{9}$$

Application of (5) to (9) transformed the phase function to range frequency-Doppler domain as in (10). Subsequently applying (7), the target velocity phase refocusing function is able to be illustrated as (11)

$$\varphi_2\left(f_\tau, f_\eta\right) = \frac{\pi\lambda_0}{2\left(1 + \frac{\lambda_0 f_\tau}{c_0}\right)}\frac{R_0}{(v_a - v_x)^2}f_\eta^2 \tag{10}$$

$$\varphi_{\text{comp}}\left(f_\tau, f_\eta\right) = \frac{\pi\lambda_0 R_0}{2\left(1 + \frac{\lambda_0 f_\tau}{c_0}\right)}\left(\frac{1}{v_a^2} - \frac{1}{(v_a - v_x)^2}\right)f_\eta^2. \tag{11}$$

The largest difference between conventional phase refocusing and the proposed refocusing was the generation of intentionally defocused SAR images with identical dimensions of SLC with respect to different target azimuth velocities. Conventional refocusing algorithms such as PGA, ISAR ME autofocusing, and MD refocusing uniquely developed well-focused image while compensating global phase distortion, while velocity-induced phase distortion was able to be mitigated in target chip or subaperture image [19], [20], [21]. Exploiting the advantage of the proposed velocity refocusing, intentionally defocused SAR images were made using (11), which were used to develop a robust vessel detection algorithm to defocused moving vessels. The proposed target velocity SAR phase refocusing function was applied to ICEYE SAR spotlight satellite images, the specification of which is illustrated in Table I.

TABLE I
ICEYE SAR DATA SPECIFICATION

Radar Sensor Parameter	Notation	Value
Center Frequency	f_c	9.65×10^9 Hz
Chirp Bandwidth	BW	3.0×10^8 Hz
Pulse Repetition Frequency (approx.)	PRF	6200 Hz (Acquisition) 38000 Hz (Processing)
Polarization	-	VV
Incidence Angle	θ_i	$20 - 35°$
Resolution (Single Look)	-	0.5 m (Range) 0.25 m (Azimuth)
Swath Width, Length	-	5 km × 5 km

III. METHODOLOGY

In order to effectively recognize the vessels in the SAR image, mitigation of the velocity-distorted phase was highly required. In advance, the target data to be refocused should be detected, which requires a large quantity of training data, including defocused targets. Quantitative training data enhancement for vessel detection and qualitative training

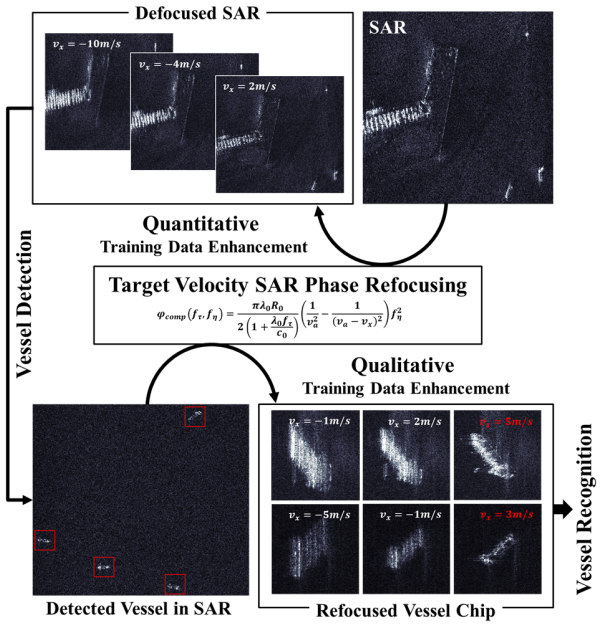

Fig. 2. Illustrated diagram of the proposed quantitative and qualitative training data enhancement of vessel training data.

data enhancement for vessel recognition were presented here, applying the proposed target velocity SAR phase refocusing function. A major contribution of the proposed algorithm was that the quantitative and qualitative enhancements were performed continuously and contributed to detection and recognition performance improvements. Fig. 2 illustrates the diagram of the quantitative and qualitative vessel training data enhancement using target velocity phase refocusing.

A. Quantitative Enhancement of Training Data and Vessel Detection

While using supervised learning in object detection, training data significantly determined its accuracy [25]. Notably, training data acquisition for vessels in the SAR images was complicated, which was often accompanied by AIS information in the corresponding scene. The algorithm developed for automatic training data acquisition from AIS information in [12] was equally applied to this study.

For SAR image after radiometric and geometric calibration, each pixel was imaged at different acquisition times [26]. As AIS information was acquired in a discrete manner, estimating the target interpolation time corresponding to each vessel was essential. This issue was resolved by introducing an iterative time interpolation; bulk interpolation on AIS-based positions was performed with respect to mean acquisition time, followed by renovating the target interpolation time to the acquisition time of the interpolated position. This performance was repeatedly performed until the movement from interpolation was bounded in a spatial resolution.

As described in (4), range projection of target velocity is caused by the target focused in an azimuth-shifted position, namely azimuth offset, which is denoted as follows [17]:

$$\delta_x = \frac{v_y y_0}{v_a}. \tag{12}$$

As proper matching between the SAR image and AIS information was able to be accomplished from correction of (12), the interpolated velocity was transformed into v_y, while the SAR state vector was exploited in the form of six orbital elements in order to derive the distance between antenna and target in geocentric coordinate [27]. After matching the vessels in the SAR image with AIS information, training data was acquired in the form of a rectangular bounding box.

Since AIS information represented verified signals from vessels, its unique application to training data acquisition was useful in mid- to low-resolution SAR images containing a number of targets. In contrast, two major limitations exist in high-resolution SAR images: 1) lack of training data in each image scene and 2) greater impact of velocity-induced phase distortion. Resolving both of the issues required data augmentation, which practically reflects the SAR signal character. Accordingly, the target velocity SAR phase refocusing presented in Section II was inversely used in order to generate defocused SAR images. In contrast to conventional data augmentation methods in object detection performed on image chips [28], [29], inversion of the refocusing function generates the SAR image with the entire SLC dimension. Training data was augmented 20 times in quantity and defocused from $v_x = -10$ m/s to $v_x = 10$ m/s with 1 m/s spacing. Generated defocused images were equally preprocessed with radiometric and geometric calibration.

ICEYE spotlight SAR images were used, whose specification denoted as in Table I. Training dataset was used to generate a vessel detection algorithm based on You Only Look Once version 4 (YOLOv4) [30]; a conventional CNN-based object detector was used without modification in order to uniquely assess the effectiveness of augmented training database. Compared to the state-of-the-art object detectors, YOLOv4 was confirmed robust to image distortion; in the case of SAR image [31], high ocean surface backscattering from wind velocity and phase distortion of targets.

Both training and validation images were normalized so that the object detector was able to recognize vessel types and small vessels. As vessel signatures had significantly higher backscattering values than ocean, data normalization was performed after bounding the maximum value of backscattering. Object detectors based on YOLO and its variations used three-band images as input [30], [31]; this study accordingly converted the single-band SAR input image into a three-band image whose maximum backscattering coefficient σ_0 was defined as 0.5, 0.7, and 1.0 for each band. The image with low maximum σ_0 aided the detection of small vessels, while that with high maximum σ_0 highlighted the vessel superstructure to assist its recognition.

Along with different vessels in SAR images and their defocused states, the vessel detection algorithm trained from them was anticipated to demonstrate robust performance on defocused moving targets.

B. Qualitative Enhancement of Training Data and Vessel Recognition

Unlike conventional autofocusing algorithms, which also targeted to remove phase defocusing from antenna motion

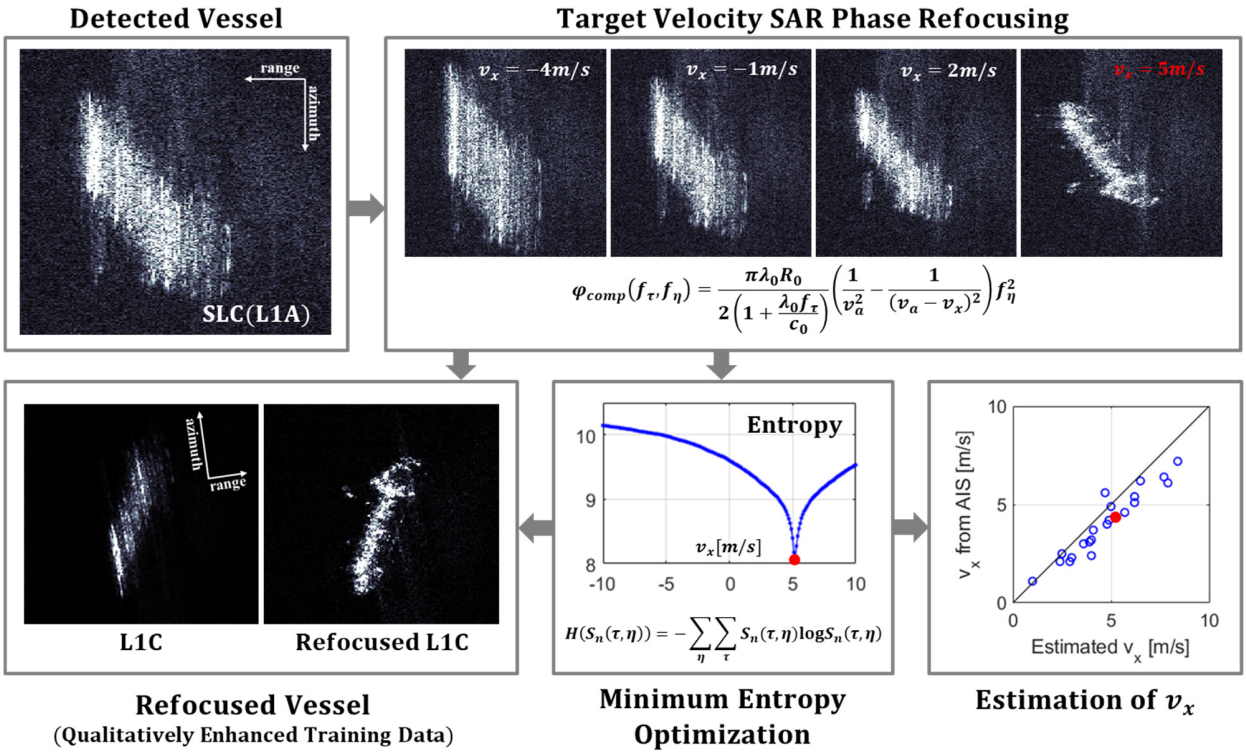

Fig. 3. Schematic illustration of the target velocity SAR phase refocusing on detected vessels for qualitative training data enhancement.

error [19], [20], [21], the proposed refocusing function was focused on eradicating the velocity-induced phase distortion as it operated an initial value problem subject to target azimuth velocity. The selection of the vessel targets on which the velocity SAR phase refocusing was performed was, therefore, spatially restricted to the detected bounding box; moreover, using the effective assessment parameter, which determines the well-focused SAR signature, was essential.

Vessel refocusing was performed by cropping the detected target vessel in defocused images with respect to different azimuth velocities while selecting the best-focused image using Entropy. Widely used in autofocusing, Entropy was defined as a parameter indicating randomness; low Entropy signifies the energy concentrated to a small number of pixels, and therefore, well-focused [32]. For the normalized intensity of SAR SLC image S_n, Entropy is defined as follows:

$$H(S_n(\tau,\eta)) = -\sum_{\eta}\sum_{\tau} S_n(\tau,\eta)\log S_n(\tau,\eta). \tag{13}$$

With spacing of 0.1 m/s, target azimuth velocity ranging from $v_x = -10$ m/s to $v_x = 10$ m/s was used in order to generate velocity-defocused SLC images from which the detected vessels were selected. After the SLC image generation was terminated, the vessel chip with the lowest Entropy and azimuth velocity corresponding to it were both selected. While the refocused vessel chips were used as qualitatively enhanced training data, the velocity was measured as estimated azimuth velocity from SAR phase distortion. The detailed illustration of the proposed refocusing application is described in Fig. 3.

After the qualitative enhancement of detected vessels, a new focused SLC image was transformed into a calibrated and geocoded SAR image before being used as training data for vessel recognition; nevertheless, as effective vessel recognition required a well-focused high-resolution image [33], it was impossible to quantitatively expand the dataset unlike that of vessel detection. The number of classes in recognition, moreover, additionally reduced training data quantity; the types of vessels were marked as double-digit numbers in AIS information with 100 different classes [12].

Several studies aimed to recognize vessels with respect to their length under the lack of training data [34], [35], [36]. In contrast, the practical application of vessel monitoring from remotely sensed data required the estimation of vessel type and its velocity. Accordingly, in order to ascertain the effect of qualitative training data enhancement on vessel recognition, 100 different types of vessels were necessary to be rearranged into a small number of groups; vessels demonstrating similar backscattering patterns were assembled into similar classes. The structural similarity index (SSIM) was used in order to compare the similarity between different gray-scaled images [37]. SSIM between two different gray-scaled images I_1 and I_2 is denoted as (14), where the notations σ and μ signify the standard deviation and mean value of each image. The notation $\sigma_{I_1 I_2}$ denotes cross covariance of images I_1 and I_2. Ranging from 0 to 1, a higher value of SSIM indicated similar image patterns

$$\mathrm{SSIM}(I_1, I_2) = \frac{4\mu_{I_1}\mu_{I_2}\sigma_{I_1 I_2}}{(\mu_{I_1}^2+\mu_{I_2}^2)(\sigma_{I_1}^2+\sigma_{I_2}^2)}. \tag{14}$$

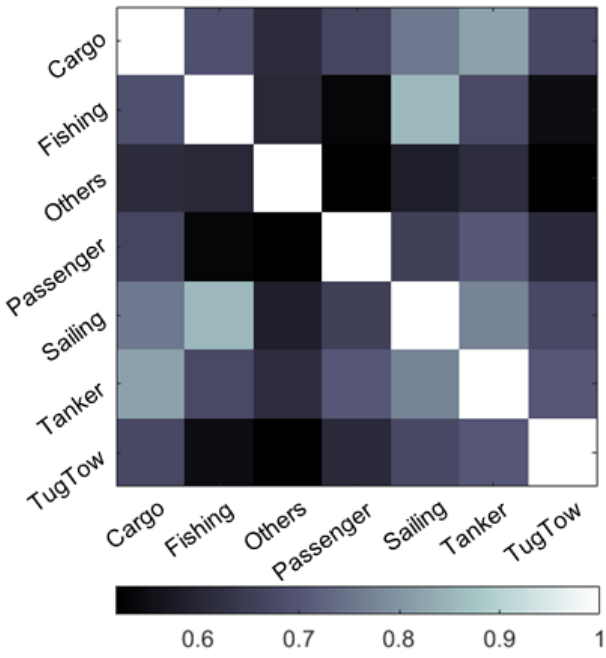

Fig. 4. Average of two SSIM comparisons between seven vessel types normalized with respect to diagonal components in row and column. Higher value of SSIM signifies greater similarity between two vessel categories.

SAR images used in vessel recognition were acquired from the western coast of South Korea. According to corresponding AIS information, six vessel types with more than ten vessels within its type were selected: cargo vessels, fishing vessels, passenger vessels, sailing vessels, tanker, and tug-towing vessels, while the other types of vessels were sorted together in a single class. Among seven different vessel types, five vessels from each type were randomly selected, aligned to identical headings and resized to 100×100 pixels from SAR images after geocoding. In addition, SSIM was estimated for all possible pairs of two different vessel types, followed by averaging the values for each class.

SSIM values were normalized with respect to column and row and averaged for effective comparison between different vessel types. Fig. 4 describes the SSIM values after normalizing and averaging. The high value of similarity was observed in classes of cargo and tanker vessesl, fishing vessels, and sailing vessels. Accordingly, the vessels were rearranged into three different classes: 1) cargo and tanker, 2) fishing vessels and sailing vessels, and 3) all the other types of vessels. The detector used in vessel detection was identically applied, only adding the function of multiclass detection in order to assess the performance in similar conditions. Preprocessing of ICEYE SAR images for vessel recognition was conducted equally to that of vessel detection.

IV. Results

Consecutive investigation on the effects of quantitative and qualitative enhancement of training data was presented in this section, analyzing vessel detection and recognition results. Assessment of vessel detection using quantitative training data enhancement was performed initially, followed by vessel recognition with respect to three different classes. Training and validation data from ICEYE SAR spotlight images were used separately for vessel detection and recognition. For vessel detection, 17 SAR images with 123 vessels were used, whose quantity was expanded 20 times. Accordingly, the vessel detector was validated using four SAR images with 63 vessels; moreover, the vessel detector was applied to 16 SAR images, detecting 216 vessels; 12 images with 153 vessels were used for recognition model training and four images with 63 vessels were used for validation.

The performance of the vessel detector was evaluated following that of a conventional object detector, applying three different parameters: precision, recall, and F1 [38]. Precision and recall, respectively, estimate the accuracy of a detector with respect to the detection performance itself and ground truth data as denoted in (15) and (16); nevertheless, overall detection accuracy was often evaluated by F1, which was defined as a harmonic average between precision and recall as in (17), given the trade-off relation of precision and recall. In (15)–(17), notations n_{ac}, n_d, and n_g, respectively, signify the number of accurate detection, total detection, and ground

TABLE II
Vessel Detection Performance on Four ICEYE SAR Images Using Quantitatively Enhanced Training Data

Acquisition	Precision	Recall	F1
Overall	**91.04%**	**96.82%**	**93.84%**
13/12/2021 17:19:12	94.11%	94.11%	94.11%
18/12/2021 12:52:39	87.50%	93.33%	90.32%
21/12/2021 04:42:52	90.91%	100%	95.24%
21/12/2021 12:20:42	91.67%	100%	95.65%
Acquisition	n_{ac}	n_d	n_g
Overall	**61**	**67**	**63**
13/12/2021 17:19:12	16	17	17
18/12/2021 12:52:39	14	16	15
21/12/2021 04:42:52	11	12	11
21/12/2021 12:20:42	20	22	20

TABLE III
Vessel Detection Performance (Recall) on Moving Vessels

Acquisition	n_{ac}	n_g	Recall
Overall	**30**	**31**	**96.77%**
13/12/2021 17:19:12	12	12	100%
18/12/2021 12:52:39	6	7	85.71%
21/12/2021 04:42:52	2	2	100%
21/12/2021 12:20:42	10	10	100%

TABLE IV
VESSEL RECOGNITION PERFORMANCE ON FOUR ICEYE SAR IMAGES USING QUALITATIVELY ENHANCED TRAINING DATA

Dataset	Acquisition	Class	Precision	Recall	F1	n_{ac}	n_d	n_g
Before Qualitative Enhancement	**Overall**	**Total**	**64.29%**	**71.43%**	**67.67%**	**45**	**70**	**63**
		I	**37.50%**	**25.00%**	**30.00%**	**3**	**8**	**12**
		II	**72.92%**	**85.37%**	**78.65%**	**35**	**48**	**41**
		III	**50.00%**	**70.00%**	**58.33%**	**7**	**14**	**10**
	30/04/2022 17:27:35	I	100%	50.00%	66.67%	1	1	2
		II	83.33%	100%	90.91%	10	12	10
		III	-	-	-	0	0	2
	06/05/2022 17:32:39	I	-	-	-	0	2	4
		II	68.75%	91.67%	78.57%	11	16	12
		III	-	-	-	0	1	0
	10/05/2022 01:11:42	I	50.00%	25.00%	33.33%	1	2	4
		II	63.64%	87.50%	73.68%	7	11	8
		III	54.55%	100%	70.58%	6	11	6
	12/05/2022 01:31:48	I	33.33%	50.00%	40.00%	1	3	2
		II	77.78%	63.64%	70.00%	7	9	11
		III	50.00%	50.00%	50.00%	1	2	2
After Qualitative Enhancement	**Overall**	**Total**	**80.00%**	**82.53%**	**81.25%**	**52**	**65**	**63**
		I	**77.78%**	**58.33%**	**66.67%**	**7**	**9**	**12**
		II	**82.61%**	**92.68%**	**87.36%**	**38**	**46**	**41**
		III	**70.00%**	**70.00%**	**70.00%**	**7**	**10**	**10**
	30/04/2022 17:27:35	I	-	-	-	0	1	2
		II	75.00%	90.00%	81.82%	9	12	10
		III	-	-	-	0	0	2
	06/05/2022 17:32:39	I	100%	75.00%	85.71%	3	3	4
		II	85.71%	100%	92.31%	12	14	12
		III	-	-	-	0	0	0
	10/05/2022 01:11:42	I	100%	50.00%	66.67%	2	2	4
		II	72.73%	100%	84.21%	8	11	8
		III	66.67%	100%	80.00%	6	9	6
	12/05/2022 01:31:48	I	66.67%	100%	80.00%	2	3	2
		II	100%	81.82%	90.00%	9	9	11
		III	100%	50.00%	66.67%	1	1	2

truth

$$Pr = \frac{n_{\text{ac}}}{n_d} \tag{15}$$

$$Re = \frac{n_{\text{ac}}}{n_g} \tag{16}$$

$$F1 = \frac{2PrRe}{Pr + Re}. \tag{17}$$

The determination on object detection was made by estimating intersection-over-union (IoU) between two different types of bounding boxes: ground truth bounding box from AIS information and that from detection. As the name suggested, IoU was defined as a ratio between the areas of intersection over that of union; following [15] and [39], bounding box pairs demonstrating IoU over 0.2 were regarded as accurately detected vessels.

Table II denotes the vessel detection performances tested on four ICEYE SAR SLC image datasets after using quantitative training data enhancement. Applying the vessel detector to SLC images after radiometric and geometric calibration deduced 91.04% precision, 96.82% recall, and 93.84% F1 overall: 61 vessels were regarded as accurate detection among 67 detection and 63 ground truth data in total. Table III illustrates the detection performance targeted to vessels with significant velocity, faster than 1 m/s ascertained using AIS information and the proposed target velocity SAR phase refocusing. According to Table III, the detection performance of moving vessels derived 96.77% of recall, which demonstrated similar results to recall in Table II.

Table IV describes the vessel recognition performance on three different categories rearranged as in Fig. 4, where class I, II, and III, respectively, signify cargo-tanker, fishing vessels-sailing vessels and the other types of vessels. Overall performance of vessel recognition augmented from 64.29% of precision, 71.43% of recall, and 67.67% of F1 score before phase refocusing to 80.00% of precision, 82.53% of recall, and 81.25% of F1 score after refocusing. The emptied spaces in

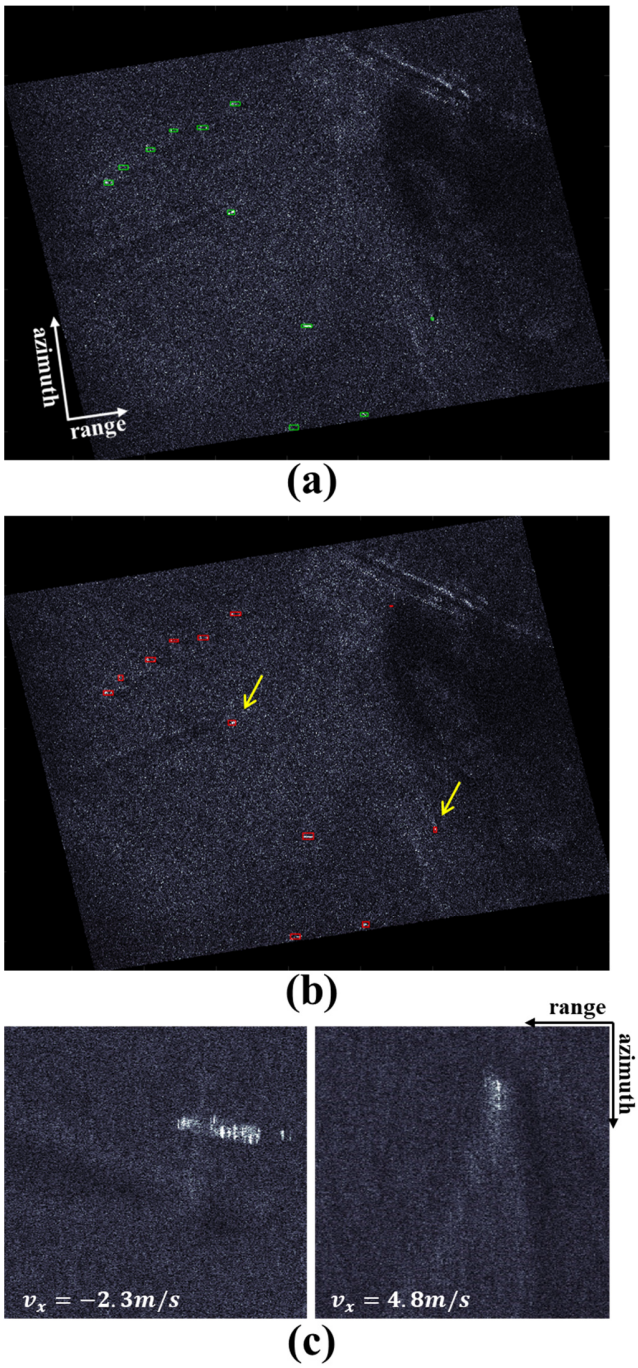

Fig. 5. Vessel detection using quantitatively enhanced training data on ICEYE SAR image: (a) ground truth acquired on 21/12/2021 04:42:52, (b) detection results, and (c) detected defocused moving vessels in SLC image with their azimuth velocities. Yellow arrow pointers in (b) indicate the moving vessels in (c).

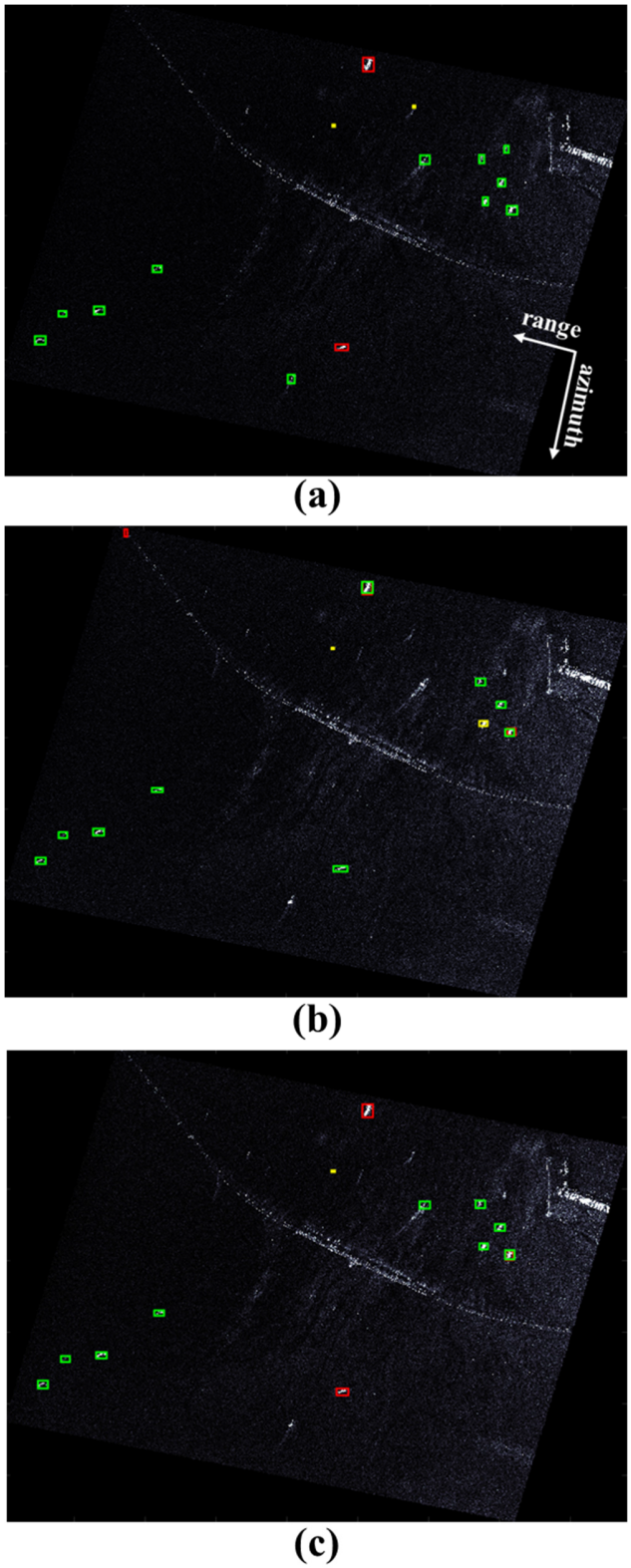

Fig. 6. Vessel recognition on ICEYE SAR image acquired on 12/05/2022 01:31:48, (a) ground truth, (b) detection before phase refocusing, and (c) detection after phase refocusing. Red, green, and yellow bounding boxes, respectively, signify the categorized class of cargo and tanker vessels, fishing and sailing vessels, and other types of vessels.

Table IV signify that no accurate recognition is found for that condition. Figs. 5 and 6, respectively, illustrate the example result on vessel detection and recognition.

V. Discussion

A number of studies on vessel monitoring focused on performance enhancement from modifying and comparing different detection algorithms [9], [10], [14], [15]. When it came to using detectors based on artificial intelligence, however, quantity and quality of training data were decisive in their accuracy [28]. Although the quantitative enhancement was studied in form of obtaining training data from

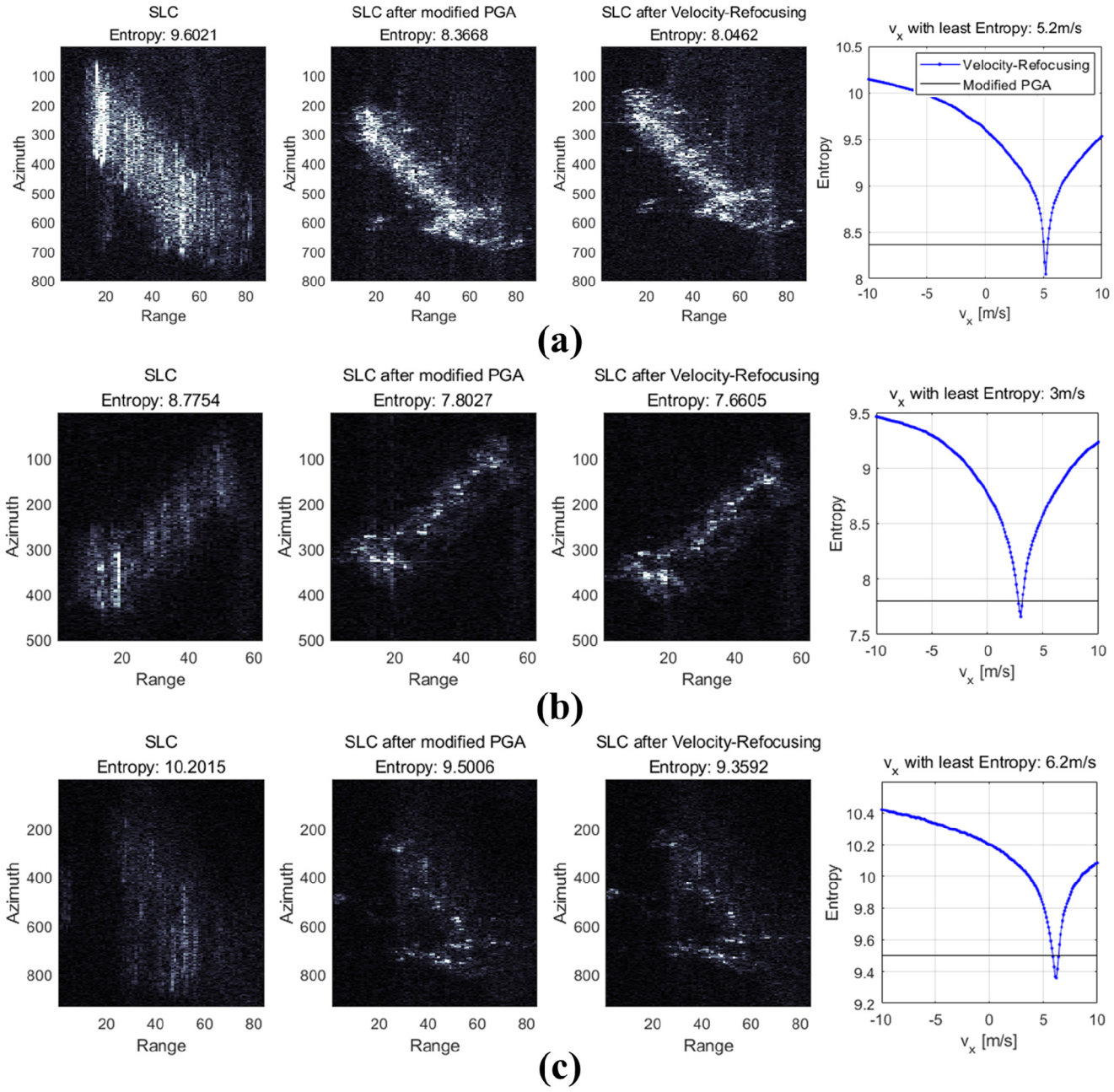

Fig. 7. Example of three different vessels (a)–(c) of applying modified PGA and the proposed target velocity refocusing algorithm.

AIS information [11], [12], acquiring training data from high-resolution SAR images with small number of vessels was still challenging. In addition, phase distortion caused by moving target azimuth velocity decreased the competence of vessel recognition. The main originality of this study was to perform vessel recognition properly using high-resolution SAR images, consecutively performed from robust detection of vessels and their refocusing applying a target velocity SAR phase refocusing function.

From Tables II to III, vessel detection using quantitatively enhanced training data of vessel demonstrated a robust detection performance regardless of moving target phase distortion. It was able to be implied that the robustness of vessel detection was ensured due to the various conditions of the moving vessels with distorted phase. In addition, Table IV indicated significant vessel recognition performance improvement after SAR phase refocusing, ascertaining the qualitative vessel training data enhancement was effective in their recognition.

Phase distortion due to antenna motion error and target velocity was conventionally compensated from PGA [19]. As a nonparametric focusing algorithm, PGA does not require any initial value for autofocusing. Before its operation, a chip was selected from the SAR image, including the defocused target; if not PGA only calibrates the defocusing from antenna motion, which was negligible in the satellite SAR system [19]. For each selected chip, the brightest scatterer in its range profile was aligned to the range center. Accordingly, scatterers were windowed, assuming the distribution of weak targets as

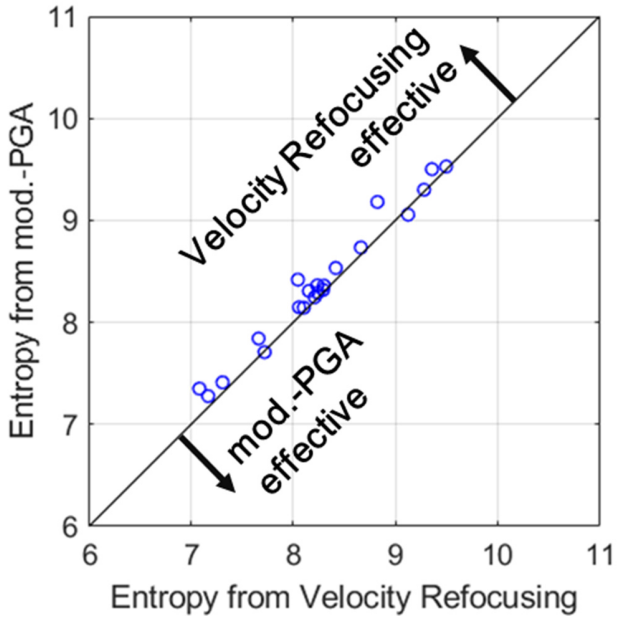

Fig. 8. Comparison of focusing competence between the modified PGA and the proposed target velocity refocusing algorithm.

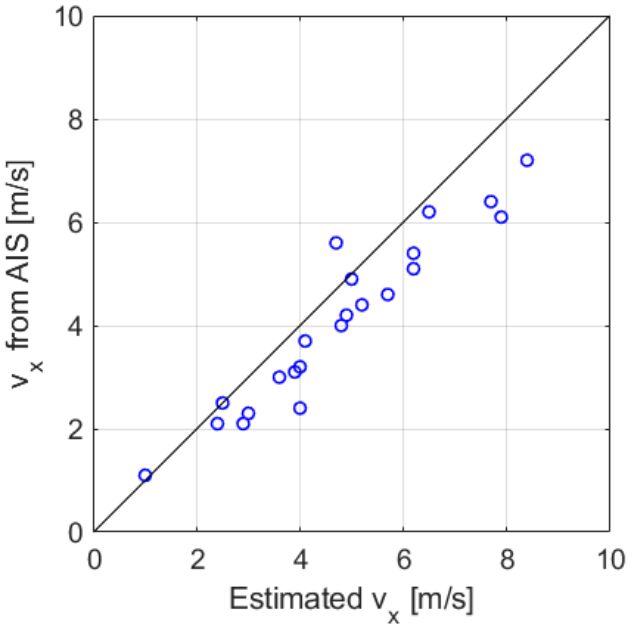

Fig. 9. Comparison between estimated azimuth velocity from the proposed refocusing algorithm and AIS-driven azimuth velocity. Average azimuth velocity offset was measured as 0.68 m/s, with a standard deviation of 0.59 m/s.

Gaussian noise [40]. Phase gradient was estimated and used to calibrate the phase error repeatedly, subsequently deriving the focused image chip after several iterations. Given the continuous enhancement of PGA, a modified PGA algorithm, which used the weighted phase gradient estimation was used as a reference focusing algorithm [41]. Exploiting the normalized signal-to-clutter ratio weight, modified PGA enabled to intensify the contribution from significant targets, which accordingly enhanced the performance of phase refocusing compared to that of conventional PGA.

Modified PGA was equally applied to the detected vessel chips along with the proposed target velocity SAR phase refocusing. PGA and its variations were operated until the phase error difference is reduced below a user-defined threshold [19]. A new decision rule was adopted for comparison with the proposed target velocity SAR phase refocusing algorithm; modified PGA was conducted for 100 iterations and finally evaluated using Entropy as in (13). Fig. 7 illustrates the examples of vessel refocusing from PGA and the proposed refocusing, while Fig. 8 describes their Entropy. It was demonstrated that the proposed target velocity refocusing algorithm outperformed the modified PGA in refocusing vessels with a satellite SAR system.

Accurate estimation of phase gradient was limited when the Gaussian noise assumption was unsuitable [40], especially when strong targets were aligned and concentrated in vicinity. This was a typical case of a vessel imaged by satellite SAR, as the superstructure of the vessel generated intensive backscattering [42]. Accordingly, it was able to be determined that the proposed target velocity refocusing algorithm is more appropriate for vessel refocusing using satellite SAR system.

The estimation of vessel azimuth velocity, which reduces Entropy to the least was performed using (11). Vessels with significant azimuth velocity ($v_x > 1\text{m/s}$) were selected and accordingly tested against v_x derived from preprocessed AIS information. Fig. 9 describes the comparison between the estimated v_x from SAR and that derived from AIS information. Average azimuth velocity offset was measured as 0.68 m/s, which significantly outperformed those from previous studies based on Doppler rate measurement using fractional Fourier Transform: 1.29 m/s [43] and 1.33 m/s [44].

For azimuth velocity estimation, the proposed algorithm assumed the effect of range velocity and acceleration to phase distortion was negligible while deriving (3) from (2). In order to ascertain whether the assumption was valid, the significance of range velocity and acceleration over the SAR SLC phase was quantified. Given the derivation of (11), it was possible to deduce the SAR phase compensation signal, including range velocity and acceleration. Phase compensation signals are described as in (18)–(21): only considering azimuth velocity (18), adding range velocity (19), adding range acceleration (20), and adding both range velocity and acceleration (21), respectively,

$$S_{c,1}(f_\tau, f_\eta) = \exp\left[-j\frac{\pi\lambda_0 R_0}{2\left(1+\frac{\lambda_0 f_\tau}{c_0}\right)}\left(\frac{1}{v_a^2}-\frac{1}{(v_a-v_x)^2}\right)f_\eta^2\right] \tag{18}$$

$$S_{c,2}(f_\tau, f_\eta) = \exp\left[-j\frac{\pi\lambda_0 R_0}{2\left(1+\frac{\lambda_0 f_\tau}{c_0}\right)}\left(\frac{1}{v_a^2}-\frac{1}{(v_a-v_x)^2+v_y^2\left(1-\frac{y_0^2}{R_0^2}\right)}\right)f_\eta^2\right] \tag{19}$$

$$S_{c,3}(f_\tau, f_\eta)$$

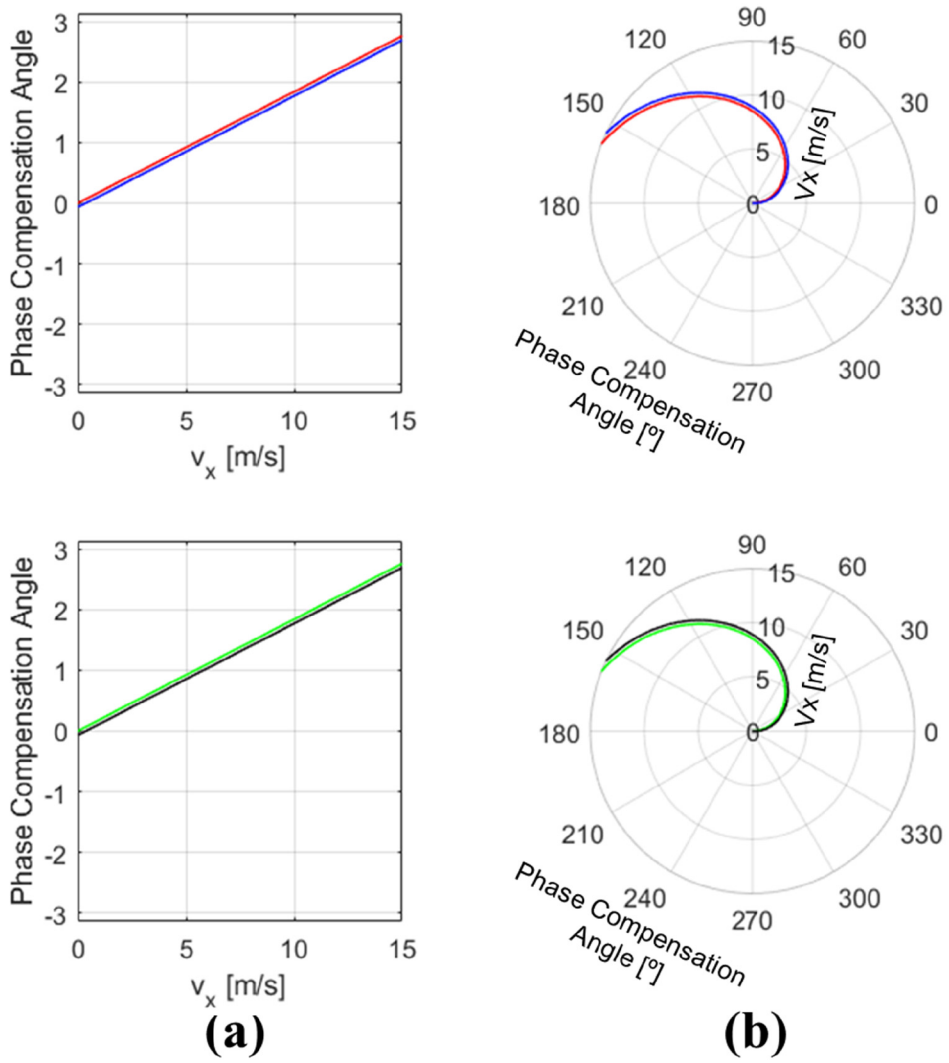

Fig. 10. Sensitivity of the target velocity phase refocusing function with respect to azimuth velocity in (a) Cartesian and (b) polar coordinate with $v_y = 7\text{m/s}$ and $a_y = 0.02\text{m/s}^2$. Red, green, blue, and black lines, respectively, denote the loci of (18), (19), (20), and (21). Simulation was performed in accordance with ICEYE satellite SAR system. Red-green and blue-black loci demonstrate identical paths with each other.

$$= \exp\left[-j\frac{\pi\lambda_0 R_0}{2\left(1+\frac{\lambda_0 f_\tau}{c_0}\right)}\left(\frac{1}{v_a^2}-\frac{1}{(v_a-v_x)^2+y_0 a_y}\right)f_\eta^2\right] \tag{20}$$

$$S_{c,4}(f_\tau, f_\eta) = \exp\left[-j\frac{\pi\lambda_0 R_0}{2\left(1+\frac{\lambda_0 f_\tau}{c_0}\right)}\left(\frac{1}{v_a^2}-\frac{1}{(v_a-v_x)^2+v_y^2\left(1-\frac{y_0^2}{R_0^2}\right)+y_0 a_y}\right)f_\eta^2\right]. \tag{21}$$

Using (18)–(21), four different SAR simulations were performed using the geometry and specifications of ICEYE satellite SAR as described in Table I. In addition, target motion was equally assumed as $v_y = 7$ m/s and $a_y = 0.02$ m/s^2, which were larger than any other vessel in the acquisition scene. Simulation results of phase compensation angle with respect to different azimuth velocities are illustrated in Fig. 10. In accordance with Fig. 10, range velocity did not influence phase distortion, whereas range acceleration effect was insignificant; 0.07 radian of phase angle difference was estimated from the fastest acceleration possible in the scene. It clearly supported that the elimination of range velocity and acceleration from the derivation of (11) was valid. It demonstrated that vessel velocity estimation is possible from the proposed phase refocusing function without using wake signatures to measure azimuth offset [45], [46], [47].

Conventional vessel monitoring using remotely sensed data was frequently aimed to detect vessels in low-resolution satellite images due to the lack of training data [12], [48]. In contrast to the increasing demand of vessel detection and recognition using high-resolution SAR images, their practical enhancements were yet to be performed. The target velocity SAR phase refocusing algorithm proposed in this study not only demonstrated the high competence of phase focusing over the conventional autofocusing algorithm using accurate velocity measurement but also enabled the training data augmentation by generating the defocused SAR image in entire SLC dimension. By exploiting both advantages, the velocity refocusing algorithm was able to be applied to realistic vessel

surveillance in the ocean, as vessel detection, recognition, and velocity estimation were sequentially performed.

Previous autofocusing algorithms were mostly applied to selected targets rather than the entire scene. Operation of PGA-based algorithms, particularly, did not require any input variable or parameter related to acquisition geometry [19], [40]. Although applying autofocusing on the target was able to be efficient in time, it did not completely assess the phase defocusing from azimuth velocity. By using the azimuth velocity as an initial value, the proposed refocusing was enabled to generate an intentionally defocused SAR SLC image covering the entire scene; this helps to develop a practical vessel detector in the SAR image, which includes moving vessels. SAR images containing a number of vessels in the scene were more effective when using the proposed refocusing algorithm since refocusing the entire SLC scene took much more time than selecting the well-focused chip.

This study mitigated an issue that kept the conventional vessel defocusing from being applied to practical vessel surveillance: the detection of the vessel, which selects the region to be refocused. A quantitative training data enhancement using the target velocity SAR phase refocusing algorithm was applied and augmented the training data 20 times in order to generate a robust detector on the defocused vessel; moreover, the application of the proposed algorithm for phase refocusing and velocity estimation was effective, ascertained from low Entropy and azimuth velocity estimation offset with respect to AIS information.

VI. Conclusion

As vessel detection and recognition were both essential in stable marine vessel surveillance, acquiring training data on vessels was essential in the development of robust vessel detectors in single and multiple classes. In this study, the target velocity SAR phase refocusing function was proposed and accordingly applied to quantitative and qualitative training data enhancement in order to develop a robust vessel detector and subsequent vessel recognition algorithm. In contrast to the conventional SAR refocusing, which uniquely aimed to generate a well-focused target chip, the proposed algorithm was able to generate a number of intentionally defocused SAR SLC images with respect to different azimuth velocities. Exploiting such character, training data of vessel was quantitatively expanded and accordingly generated a vessel detector robust to defocused moving vessels; furthermore, the detected vessels were refocused using the target velocity SAR phase refocusing function and used as qualitatively enhanced training data for vessel recognition. Compared to the conventional SAR refocusing algorithm and velocity estimator, the proposed target velocity SAR phase refocusing function demonstrated significantly enhanced performance in both capacities. Detection and recognition results demonstrated in this study were subject to the training data enhancement in a quantitative and qualitative manner, respectively. The assumptions made in the derivation of the target velocity SAR phase refocusing function were additionally analyzed, ascertaining the effectiveness of phase refocusing and abridging the range movement terms of the target. As consecutive vessel detection and vessel recognition were performed in this study, a robust and stable marine vessel monitoring apparatus is expected to be developed using the proposed algorithm.

Acknowledgment

The authors would like to thank the Ministry of Oceans and Fisheries (MOF), South Korea, for providing AIS data.

References

[1] Y. Wang, Z. Zhang, N. Li, F. Hong, H. Fan, and X. Wang, "Maritime surveillance with undersampled SAR," *IEEE Geosci. Remote Sens. Lett.*, vol. 14, no. 8, pp. 1423–1427, Aug. 2017.

[2] P. W. Vachon, J. W. M. Campbell, C. A. Bjerkelund, F. W. Dobson, and M. T. Rey, "Ship detection by the RADARSAT SAR: Validation of detection model predictions," *Can. J. Remote Sens.*, vol. 23, no. 1, pp. 48–59, Mar. 1997.

[3] X. Leng, K. Ji, K. Yang, and H. Zou, "A bilateral CFAR algorithm for ship detection in SAR images," *IEEE Geosci. Remote Sens. Lett.*, vol. 12, no. 7, pp. 1536–1540, Jul. 2015.

[4] W. An, C. Xie, and X. Yuan, "An improved iterative censoring scheme for CFAR ship detection with SAR imagery," *IEEE Trans. Geosci. Remote Sens.*, vol. 52, no. 8, pp. 4585–4595, Aug. 2014.

[5] Z. Zhang, H. Wang, F. Xu, and Y.-Q. Jin, "Complex-valued convolutional neural network and its application in polarimetric SAR image classification," *IEEE Trans. Geosci. Remote Sens.*, vol. 55, no. 12, pp. 7177–7188, Dec. 2017.

[6] L. Qi et al., "Ship target detection algorithm based on improved faster R-CNN," *Electronics*, vol. 8, no. 9, p. 959, Aug. 2019.

[7] T. Zhang and X. Zhang, "High-speed ship detection in SAR images based on a grid CNN," *Remote Sens.*, vol. 11, no. 10, May 2019, Art. no. 1206.

[8] R. Touzi, A. Lopes, J. Bruniquel, and P. W. Vachon, "Coherence estimation for SAR imagery," *IEEE Trans. Geosci. Remote Sens.*, vol. 37, no. 1, pp. 135–149, Jan. 1999.

[9] Z. Zhao, K. Ji, X. Xing, H. Zou, and S. Zhou, "Ship surveillance by integration of space-borne SAR and AIS – review of current research," *J. Navigat.*, vol. 67, no. 1, pp. 177–189, Jan. 2014.

[10] G. Tang, Y. Zhuge, C. Claramunt, and S. Men, "N-YOLO: A SAR ship detection using noise-classifying and complete-target extraction," *Remote Sens.*, vol. 13, no. 5, Feb. 2021, Art. no. 871.

[11] L. Huang et al., "OpenSARShip: A dataset dedicated to Sentinel-1 ship interpretation," *IEEE J. Sel. Topics Appl. Earth Observ. Remote Sens.*, vol. 11, no. 1, pp. 195–208, Jan. 2018.

[12] J. Song, D.-J. Kim, and K.-M. Kang, "Automated procurement of training data for machine learning algorithm on ship detection using AIS information," *Remote Sens.*, vol. 12, no. 9, May 2020, Art. no. 1443.

[13] J.-I. Hwang and H.-S. Jung, "Automatic ship detection using the artificial neural network and support vector machine from X-band SAR satellite images," *Remote Sens.*, vol. 10, no. 11, Nov. 2018, Art. no. 1799.

[14] J.-I. Hwang, S.-H. Chae, D. Kim, and H.-S. Jung, "Application of artificial neural networks to ship detection from X-band Kompsat-5 imagery," *Appl. Sci.*, vol. 7, no. 9, Sep. 2017, Art. no. 961.

[15] J. Ding, B. Chen, H. Liu, and M. Huang, "Convolutional neural network with data augmentation for SAR target recognition," *IEEE Geosci. Remote Sens. Lett.*, vol. 13, no. 3, pp. 364–368, Mar. 2016.

[16] R. Pelich, N. Longépé, G. Mercier, G. Hajduch, and R. Garello, "Vessel refocusing and velocity estimation on SAR imagery using the fractional Fourier transform," *IEEE Trans. Geosci. Remote Sens.*, vol. 54, no. 3, pp. 1670–1684, Mar. 2016.

[17] D.-J. Kim, W. M. Moon, D. Moller, and D. A. Imel, "Measurements of ocean surface waves and currents using l- and C-band along-track interferometric SAR," *IEEE Trans. Geosci. Remote Sens.*, vol. 41, no. 12, pp. 2821–2832, Dec. 2003.

[18] R. Scheiber and M. V. Kempen, "AIS assisted identification and refocusing of ships in airborne SAR images," in *Proc. 12th Eur. Conf. Synth. Aperture Radar (EUSAR)*, Aachen, Germany, 2018, pp. 1–4.

[19] D. E. Wahl, P. H. Eichel, D. C. Ghiglia, and C. V. Jakowatz, "Phase gradient autofocus—A robust tool for high resolution SAR phase correction," *IEEE Trans. Aerosp. Electron. Syst.*, vol. 30, no. 3, pp. 827–835, Jul. 1994.

[20] J. Wang, D. Kasilingam, X. Liu, and Z. Zhou, "ISAR minimum-entropy phase adjustment," in *Proc. IEEE Radar Conf.*, Philadelphia, PA, USA, Apr. 2004, pp. 197–200, doi: 10.1109/NRC.2004.1316421.

[21] G. Wang, M. Zhang, Y. Huang, L. Zhang, and F. Wang, "Robust two-dimensional spatial-variant map-drift algorithm for UAV SAR autofocusing," *Remote Sens.*, vol. 11, no. 3, Feb. 2019, Art. no. 340.

[22] Y. L. Neo, F. H. Wong, and I. G. Cumming, "Processing of azimuth-invariant bistatic SAR data using the range Doppler algorithm," *IEEE Trans. Geosci. Remote Sens.*, vol. 46, no. 1, pp. 14–21, Jan. 2008.

[23] K. Aberman and Y. C. Eldar, "Sub-nyquist SAR via Fourier domain range-Doppler processing," *IEEE Trans. Geosci. Remote Sens.*, vol. 55, no. 11, pp. 6228–6244, Nov. 2017.

[24] I. Cumming and F. Wong, *Digital Processing of Synthetic Aperture Radar Data: Algorithms and Implementation*. Norwood, MA: Artech House, 2005.

[25] J. Han, D. Zhang, G. Cheng, N. Liu, and D. Xu, "Advanced deep-learning techniques for salient and category-specific object detection: A survey," *IEEE Signal Process. Mag.*, vol. 35, no. 1, pp. 84–100, Jan. 2018.

[26] R. Hostache, P. Matgen, G. Schumann, C. Puech, L. Hoffmann, and L. Pfister, "Water level estimation and reduction of hydraulic model calibration uncertainties using satellite SAR images of floods," *IEEE Trans. Geosci. Remote Sens.*, vol. 47, no. 2, pp. 431–441, Feb. 2009.

[27] P. Sengupta, S. R. Vadali, and K. T. Alfriend, "Satellite orbit design and maintenance for terrestrial coverage," *J. Spacecraft Rockets*, vol. 47, no. 1, pp. 177–187, Jan. 2010.

[28] Z. Suo, Y. Zhao, S. Chen, and Y. Hu, "BoxPaste: An effective data augmentation method for SAR ship detection," *Remote Sens.*, vol. 14, no. 22, Nov. 2022, Art. no. 5761.

[29] Z. Wang, L. Du, J. Mao, B. Liu, and D. Yang, "SAR target detection based on SSD with data augmentation and transfer learning," *IEEE Geosci. Remote Sens. Lett.*, vol. 16, no. 1, pp. 150–154, Jan. 2019.

[30] A. Bochkovskiy, C.-Y. Wang, and H.-Y. Mark Liao, "YOLOv4: Optimal speed and accuracy of object detection," 2020, *arXiv:2004.10934*.

[31] W. Yuan, D. Choi, D. Bolkas, P. H. Heinemann, and L. He, "Sensitivity examination of YOLOv4 regarding test image distortion and training dataset attribute for apple flower bud classification," *Int. J. Remote Sens.*, vol. 43, no. 8, pp. 3106–3130, Jun. 2022.

[32] T. Zeng, R. Wang, and F. Li, "SAR image autofocus utilizing minimum-entropy criterion," *IEEE Geosci. Remote Sens. Lett.*, vol. 10, no. 6, pp. 1552–1556, Nov. 2013.

[33] H. Zhang, X. Zhang, G. Meng, C. Guo, and Z. Jiang, "Few-shot multi-class ship detection in remote sensing images using attention feature map and multi-relation detector," *Remote Sens.*, vol. 14, no. 12, Jun. 2022, Art. no. 2790.

[34] G. Liu, Y. Zhang, X. Zheng, X. Sun, K. Fu, and H. Wang, "A new method on inshore ship detection in high-resolution satellite images using shape and context information," *IEEE Geosci. Remote Sens. Lett.*, vol. 11, no. 3, pp. 617–621, Mar. 2014.

[35] S. Li, Z. Zhou, B. Wang, and F. Wu, "A novel inshore ship detection via ship head classification and body boundary determination," *IEEE Geosci. Remote Sens. Lett.*, vol. 13, no. 12, pp. 1920–1924, Dec. 2016.

[36] L. Chen, W. Shi, and D. Deng, "Improved YOLOv3 based on attention mechanism for fast and accurate ship detection in optical remote sensing images," *Remote Sens.*, vol. 13, no. 4, Feb. 2021, Art. no. 660.

[37] Z. Wang, A. C. Bovik, H. R. Sheikh, and E. P. Simoncelli, "Image quality assessment: From error visibility to structural similarity," *IEEE Trans. Image Process.*, vol. 13, no. 4, pp. 600–612, Apr. 2004.

[38] Z. Lin, K. Ji, X. Leng, and G. Kuang, "Squeeze and excitation rank faster R-CNN for ship detection in SAR images," *IEEE Geosci. Remote Sens. Lett.*, vol. 16, no. 5, pp. 751–755, May 2019.

[39] J. Song, D.-J. Kim, S. Lee, S. An, J.-H. Hwang, and J. Kim, "Geometric positioning error mitigation of SAR image in ocean utilizing AIS information," *IEEE Geosci. Remote Sens. Lett.*, vol. 20, 2023, Art. no. 4003105.

[40] H. Lee, C.-S. Jung, and K.-W. Kim, "Feature preserving autofocus algorithm for phase error correction of SAR images," *Sensors*, vol. 21, no. 7, Mar. 2021, Art. no. 2370.

[41] H. Zeng, W. Yang, P. Wang, and J. Chen, "A modified PGA for spaceborne SAR scintillation compensation based on the weighted maximum likelihood estimator and data division," *IEEE J. Sel. Topics Appl. Earth Observ. Remote Sens.*, vol. 15, pp. 3938–3947, 2022.

[42] R. Touzi, J. Hurley, and P. W. Vachon, "Optimization of the degree of polarization for enhanced ship detection using polarimetric RADARSAT-2," *IEEE Trans. Geosci. Remote Sens.*, vol. 53, no. 10, pp. 5403–5424, Oct. 2015.

[43] J. Song, D.-J. Kim, S. An, and J. Kim, "Restoration of authentic position of unidentified vessels in SAR imagery: A deep learning based approach," *IEEE J. Sel. Topics Appl. Earth Observ. Remote Sens.*, vol. 15, pp. 1064–1078, 2022.

[44] M. Back, D. Kim, S.-W. Kim, and J.-S. Won, "Two-dimensional ship velocity estimation based on KOMPSAT-5 synthetic aperture radar data," *Remote Sens.*, vol. 11, no. 12, p. 1474, Jun. 2019.

[45] M. D. Graziano and A. Renga, "Towards automatic recognition of wakes generated by dark vessels in Sentinel-1 images," *Remote Sens.*, vol. 13, no. 10, p. 1955, May 2021.

[46] K. Ouchi, M. Iehara, K. Morimura, S. Kumano, and I. Takami, "Nonuniform azimuth image shift observed in the radarsat images of ships in motion," *IEEE Trans. Geosci. Remote Sens.*, vol. 40, no. 10, pp. 2188–2195, Oct. 2002.

[47] P. Heiselberg, K. Sørensen, and H. Heiselberg, "Ship velocity estimation in SAR images using multitask deep learning," *Remote Sens. Environ.*, vol. 288, Apr. 2023, Art. no. 113492.

[48] X. Xu, X. Zhang, and T. Zhang, "Lite-YOLOv5: A lightweight deep learning detector for on-board ship detection in large-scene Sentinel-1 SAR images," *Remote Sens.*, vol. 14, no. 4, Feb. 2022, Art. no. 1018.

Juyoung Song (Student Member, IEEE) received the B.Sc. and M.Sc. degrees in Earth and environmental sciences from Seoul National University, Seoul, Republic of Korea, in 2019 and 2021, respectively, where he is currently pursuing the Ph.D. degree in radar remote sensing and geophysics.

His research interests include vessel monitoring using synthetic aperture radar, radar signal processing, artificial intelligence, and geometric calibration of satellite images.

Duk-jin Kim (Senior Member, IEEE) received the B.Sc. degree in Earth system science and the M.Sc. and Ph.D. degrees in radar remote sensing and geophysics from Seoul National University, Seoul, South Korea, in 1999, 2001, and 2005, respectively.

From October 2005 to July 2007, he was a Post-Doctoral Researcher with the University of Manitoba, Winnipeg, MB, Canada, and with the University of Michigan, Ann Arbor, MI, USA. From July 2007 to August 2008, he was a Senior Researcher with the Remote Sensing Division, Korea Aerospace Research Institute, Daejeon, South Korea. He is currently a Full Professor with the School of Earth and Environmental Sciences, Seoul National University. During his sabbatical leave from August 2014 to July 2015, he was a Visiting Scholar with the Radar Science and Engineering Section, NASA Jet Propulsion Laboratory, California Institute of Technology, Pasadena, CA, USA. His research interests include disaster monitoring using space-borne and airborne synthetic aperture radar systems (SAR), and environmental change monitoring using multitemporal and multisource SAR data.

Prof. Kim is a member of the Korean Institute of Electromagnetic Engineering and Science, Korean Society of Remote Sensing, and the Geological Society of Korea. He participated in the Steering Committee or Advisory Committee of many satellite programs in Korea (COMS, GEO-KOMPSAT-2B, and KOMPSAT-6/8).

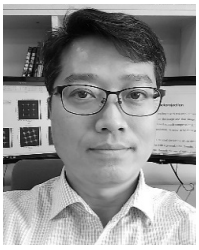

Ji-Hwan Hwang received the B.S. and M.S. degrees in radio and communication engineering and the Ph.D. degree in electronic information and communication engineering from Hongik University, Seoul, Korea, in 2001, 2003, and 2013, respectively.

He was with Mobile Communication Laboratory, LG Electronics, from 2003 to 2006, and Agilent Technologies, from 2007 to 2009, and he was with Seoul National University, Seoul, where he was a Chief Researcher at the Research Institute of Basic Science, from 2015 to 2023. Since 2023, he has been a Principal Research Engineer at the Radar Technologies Laboratory, Echo Sensing Company. His research interests include radar systems and signal processing, electromagnetic wave scattering, and microwave remote sensing.

Hwisong Kim (Student Member, IEEE) received the B.A. degree in geography education and the B.Sc. degree in Earth and environmental sciences from Korea University, Seoul, South Korea, in 2021, and the M.Sc. degree in Earth and environmental sciences from Seoul National University, Seoul, in 2023, where she is pursuing the Ph.D. degree in radar remote sensing and geophysics.

Her research interests include artificial intelligence applications using synthetic aperture radar, with interests spanning flood monitoring, target recognition, and applications in the military sector.

Chenglei Li (Student Member, IEEE) received the B.Sc. degree in geoscience and the M.Ed. degree in instructional programme (geography) from Yanbian University, Yanji, China, in 2018 and 2020, respectively. He is currently pursuing the Ph.D. degree in Earth and environmental sciences with Seoul National University, Seoul, Republic of Korea.

His research interests include marine oil spill detection, glacier calving front mapping, and coastline extraction using deep learning technologies.

Shinhye Han received the B.Eng. degree in sustainable systems engineering and computer science and engineering from Ewha Womans University, Seoul, Republic of Korea, in 2022. She is pursuing the M.Eng. degree in artificial intelligence from Seoul National University, Seoul.

Her research interests include remote sensing using synthetic aperture radar and artificial intelligence (AI)-based studies, including object detection, generative AI, and unsupervised representation learning.

Junwoo Kim received the B.Eng. degree in architecture from Yeungnam University, Gyeongbuk, South Korea, in 2011, and the M.Sc. degree in remote sensing and GIS from Kyungpook National University, Daegu, South Korea, in 2014, and the Ph.D. degree in geography from the University of Leeds, Leeds, U.K., in 2019.

He was with the Institute of Basic Sciences, Seoul National University, Seoul, South Korea, from 2019 to 2021, as a Senior Researcher, where has been a Research Professor with the SNU Future Innovation Institute, Seoul National University, since 2022. His research interests include broadening and deepening our understanding of the Earth and environments and their interactions with human beings and society, using geospatial information technologies such as remote sensing, GIS, and artificial intelligence.